frontiers in Astronomy and Space Sciences

ORIGINAL RESEARCH
published: 13 April 2021
doi: 10.3389/fspas.2021.656295

High-Resolution Infrared Spectroscopy of DC_3N in the Stretching Region

Ningjing Jiang[1], Mattia Melosso[1], Filippo Tamassia[2], Luca Bizzocchi[3], Luca Dore[1], Elisabetta Canè[2], Davide Fedele[4,5], Jean-Claude Guillemin[6] and Cristina Puzzarini[1]*

[1]Dipartimento di Chimica "Giacomo Ciamician", Università di Bologna, Bologna, Italy, [2]Dipartimento di Chimica Industriale "Toso Montanari", Università di Bologna, Bologna, Italy, [3]Center for Astrochemical Studies, Max Planck Institut für Extraterrestrische Physik, Garching bei München, Germany, [4]INAF—Osservatorio Astrofisico di Arcetri, Firenze, Italy, [5]INAF—Osservatorio Astrofisico di Torino, Pino Torinese, Italy, [6]Ecole Nationale Supérieure de Chimie de Rennes, CNRS, ISCR–UMR6226, University of Rennes, Rennes, France

The perspectives opened by modern ground-based infrared facilities and the forthcoming James Webb Telescope mission have brought a great attention to the ro-vibrational spectra of simple interstellar molecules. In this view, and because of the lack of accurate spectroscopic data, we have investigated the infrared spectrum of deuterated cyanoacetylene (DC_3N), a relevant astrochemical species. The ν_1, ν_2, and ν_3 fundamentals as well as their hot-bands were observed in the stretching region (1,500–3,500 cm^{-1}) by means of a Fourier transform infrared spectrometer. Supplementary measurements were performed at millimeter-wavelengths (243–295 GHz) with a frequency-modulation spectrometer equipped with a furnace, that allowed to probe pure rotational transitions in the investigated stretching states. Furthermore, since HC_3N is observed as by-product in our spectra and suffers from the same deficiency of accurate infrared data, its ro-vibrational features have been analyzed as well. The combined analysis of both rotational and ro-vibrational data allowed us to determine precise spectroscopic constants that can be used to model the infrared spectra of DC_3N and HC_3N. The importance of accurate molecular data for the correct modeling of proto-planetary disks and exoplanetary atmospheres is then discussed.

Keywords: cyanoacetylene, interstellar: matter, rovibrational spectroscopy, spectral analysis, infrared spectroscopy

OPEN ACCESS

Edited by:
Ryan C. Fortenberry, University of Mississippi, United States

Reviewed by:
Jennifer Van Wijngaarden, University of Manitoba, Canada
Shanshan Yu, NASA Jet Propulsion Laboratory (JPL), United States

****Correspondence:***
Mattia Melosso
mattia.melosso2@unibo.it

Specialty section:
This article was submitted to Astrochemistry, a section of the journal Frontiers in Astronomy and Space Sciences

Received: *20 January 2021*
Accepted: *16 February 2021*
Published: *13 April 2021*

Citation:
Jiang N, Melosso M, Tamassia F, Bizzocchi L, Dore L, Canè E, Fedele D, Guillemin J-C and Puzzarini C (2021) High-Resolution Infrared Spectroscopy of DC_3N in the Stretching Region. Front. Astron. Space Sci. 8:656295. doi: 10.3389/fspas.2021.656295

1 INTRODUCTION

Interstellar DC_3N was first discovered in the dark cloud TMC-1 (Taurus Molecular Cloud 1) through the observation in emission of its $J = 5 - 4$ rotational transition lying at nearly 42.2 GHz (Langer et al., 1980). Subsequently, deuterated cyanoacetylene has been extensively observed in cold molecular clouds, such as L1498, L1544, L1521B, L1400K, and L1400G (Howe et al., 1994), as well as in the hot cores of the high-mass star-forming regions Orion KL and Sagittarius B_2(N) (Esplugues et al., 2013; Belloche et al., 2016). Recently, DC_3N has been employed to investigate the evolutionary stage of massive star-forming regions: Rivilla et al. (2020) detected the emission of DC_3N ($J = 11 - 10$ transition) in a sample of 15 sources containing both cold and warm high-mass star-forming cores, and acquired the first emission map of DC_3N in the high-mass proto-cluster IRAS 05358+3543.

The astrophysical relevance of DC_3N is related both to the ubiquitous presence of its parent species (HC_3N) in Space and to its deuteration. Indeed, the study of interstellar D-containing molecules provides important information on the properties and the evolution of star-forming regions (see, e.g., Ceccarelli et al., 2014, and references therein), and is a key tool to follow the chemical history of the materials which eventually enter into the composition of planetary bodies.

On a general ground, the identification of an interstellar molecule is achieved through the detection of its rotational and/or vibrational spectral features (McGuire, 2018). In recent years, the observations of molecules in the interstellar medium (ISM) has prospered thanks to the development of new high-sensitivity telescopes operating at a wavelength range spanning from centimeter to micrometer. The Atacama Large Millimeter/sub-millimeter Array (ALMA) is one of the best facility for the observation of molecular signatures in a variety of astrophysical objects, including remote galaxies and planets. With ten different bands (from 0.32 to 3.6 mm) ALMA covers a spectral window wherein most of the rotational transitions fall, allowing to probe a multiplicity of chemical (light and medium-sized molecules) and excitation conditions (gas temperature).

On the other hand, the observation of vibrational signatures of interstellar molecules is comparatively more difficult due to the limited transparency of the Earth atmosphere in the Mid- and Far-infrared regions. Despite the fact that a number of powerful telescopes are equipped with state-of-the-art high-resolution ($R > 50,000$) infrared spectrographs (e.g., CRIRES at ESO Very Large Telescope, TEXES at NASA IR Telescope facility), still the identification of vibrational features of species different from the main tracers (H_2O, CH_4, HCN, NH_3, etc.) remains challenging due to a combination of signal weakness, line overlap, and contamination by stratospheric OH lines. In this context, a future important contribution is expected from the James Webb Space Telescope (JWST), to be launched in October 2021 as a follow-on mission of the Hubble Space Telescope. Located outside the Earth atmosphere, JWST will allow for the observation of high-sensitivity wideband infrared spectra with its on-board infrared spectrographs. The Mid-Infrared Instrument (MIRI) covers continuously the 5–28 μm region at mid resolution ($R \sim 3,000$) with four bands (Banks et al., 2008), while NIRSPEC is designed to pinpoint the shorter wavelength range (1.8–5.2 μm). Such facilities will provide a full spectral overview of the sources, thus allowing to sample simultaneously the complete vibrational manifold of the molecular targets: i.e., the bending region below 12 μm already excited in the warm gas ($T < 500$ K), and the C-H stretching region around 3 μm, characterised by high excitation energies ($E/k \sim 4,000$ K) and useful to probe the inner (AU-sized) parts of proto-planetary disks and the atmospheres of hot exoplanets.

The laboratory spectroscopic knowledge of DC_3N over the full spectral range of interest for astronomy is, however, not homogeneous. While the rotational spectrum of DC_3N has been accurately studied and it is well suited to guide astronomical observations at millimeter wavelengths, a detailed knowledge of its infrared spectrum is limited to the spectral range between 200 and 1,100 cm^{-1} (Melosso et al., 2020). At higher frequencies, only low-accuracy spectroscopic data are available in the literature (Mallinson and Fayt, 1976). The same applies to the MIR spectrum of HC_3N above 1,000 cm^{-1}, for which the ro-vibrational bands were recorded either at low resolution of 0.025 and 0.050 cm^{-1} (Mallinson and Fayt, 1976) or in a narrow spectral interval (Yamada et al., 1980; Yamada and Winnewisser, 1981; Yamada et al., 1983). Such patchy results were due mainly to the type of instrumentation employed, i.e., Ebert-type and Diode-laser spectrometers. Currently, these limitations are easily overcome by Fourier-transform infrared (FTIR) spectrometers, which offers the possibility of recording high-resolution ro-vibrational spectra in a wide frequency range.

To fill the lack of information described above, in this work we report on a comprehensive investigation of the high-resolution MIR spectra of DC_3N and HC_3N, obtained using FTIR spectroscopy. In addition, the pure rotational spectra in some vibrational excited states of DC_3N have been recorded in order to determine highly-accurate spectroscopic parameters. The new assignments of the IR and millimeter-wave spectra were combined into a single global fit from which a consistent set of spectroscopic constants has been determined. The analysis of DC_3N provides a highly-precise rest-frequency catalog useful for astronomical observations.

2 EXPERIMENTAL DETAILS

The DC_3N sample was prepared as recently reported in Melosso et al. (2020).

2.1 Fourier-Transform Infrared Interferometer

Infrared spectra of DC_3N and HC_3N were recorded in the 1,500–3,500 cm^{-1} range with a Fourier-Transform Bomem DA3.002 interferometer (Stoppa et al., 2016; Tamassia et al., 2020). In the present work, the spectrometer was equipped with a KBr beam-splitter, a Globar source, a liquid-nitrogen InSb detector, and a multipass cell whose absorption-pathlength was set to 8 m. Two spectra were recorded in the 1,500–3,500 cm^{-1} region using different pressures of DC_3N, namely 16 and 32 Pa, at a nominal resolution of 0.004 cm^{-1}. Both of them were obtained from the co-addition of 140–200 scans, for a total integration time of 13–18 h. The frequency axis of the spectra was calibrated by using some 50 transitions of H_2O and CO_2 as references, whose wavenumbers were taken from the HITRAN database (Gordon et al., 2017). On average, the calibration residuals are about 5×10^{-5} cm^{-1}. The HC_3N absorptions were also detected in the same spectra with a good signal-to-noise ratio (S/N) because of the hydrogen-deuterium (H/D) exchange occurring in the multipass cell. The line-center frequencies were retrieved with PGOPHER (Western, 2017) using the maximum intensity of the lines and their uncertainty is assumed to be 4×10^{-4} cm^{-1} in all cases.

2.2 Frequency-Modulation Millimeter/ Submillimeter-Wave Spectrometer

Pure rotational transitions of DC_3N were recorded in three high-energy vibrational states by means of a frequency-modulation (FM) millimeter/submillimeter-wave spectrometer (Melosso et al., 2019a; Melosso et al., 2019b). Briefly, the primary radiation source is a Gunn oscillator working in the W band (80–115 GHz), whose frequency is stabilized and modulated in a phase-lock loop. Higher frequencies are obtained by coupling the Gunn diode with passive frequency-multipliers (doublers and triplers). The detection system is constituted by a Schottky barrier diode connected to a lock-in amplifier set at twice the modulation frequency ($2f$ detection scheme). However, in order to observe rotational transitions belonging to vibrational states with energies between 1,900 and 2,400 cm^{-1}, a new experimental set-up has been tested. A 1.5 m long quartz absorption cell has been surrounded by a 90 cm tubular furnace capable to reach temperature as high as 1,200°C. Since the heating is not homogeneous across the whole cell, the thermally-excited molecules are most likely confined near the center of the cell, i.e., in the 90 cm directly heated by the oven. To increase the number of absorbing molecules, the spectrometer has been arranged in a double-pass configuration (Dore et al., 2012) and the effective absorption-path was at least 1.8 m. For the present measurements, the temperature furnace was set to 700°C, while a small flow (~1 Pa) of DC_3N was ensured inside the cell. The accuracy of the retrieved frequencies is estimated to be around 30 kHz.

3 ANALYSIS AND RESULTS

3.1 Theoretical Background

DC_3N is a closed shell linear molecule which possesses seven vibrational modes: four stretching modes (ν_1, ν_2, ν_3, ν_4; $\sum$ symmetry) and three doubly-degenerate bending modes (ν_5, ν_6, ν_7; $\prod$ symmetry), all of being infrared-active. The low-lying vibrational states (ν_4, ν_5, ν_6, ν_7) as well as some of their overtone and combination states have been extensively analyzed in a previous paper (Melosso et al., 2020). In the present work, we focus on the fundamental transitions of the ν_1, ν_2, and ν_3 stretching modes, and their hot bands ($\nu_1 + \nu_7 - \nu_7$, $\nu_2 + \nu_7 - \nu_7$, and $\nu_3 + \nu_7 - \nu_7$), which all lie in the MIR region. Since the corresponding bands of HC_3N, formed in the absorption cell by isotopic exchange, are visible in the same spectra, we analyzed them as well. A more extended analysis of the HC_3N data through a global fit including a large number of rotational and ro-vibrational transitions is currently being completed[1].

The effective Hamiltonian employed in this work to analyze the ro-vibrational transitions mentioned above (both DC_3N and HC_3N) and to retrieve the spectroscopic parameters was already described in Bizzocchi et al. (2017). Since the present study focuses on the analysis of three stretching states ($\sum$ symmetry) and their ν_7 associated hot bands, the Hamiltonian can be simplified as:

$$H = H_{rv} + H_{l-type} \tag{1}$$

where H_{rv} is the ro-vibrational Hamiltonian and H_{l-type} describes the l-type interaction between l sub-levels of the excited bending states.

In the ro-vibrational part, the diagonal elements of the Hamiltonian can be expressed as:

$$\begin{aligned}\langle l_7, k|H_{rv}|l_7, k\rangle &= G_v + \chi_{L(77)}l_7^2 + \left(B_v + d_{JL(77)}l_7^2\right)f(J,k) \\ &-\left(D_v + h_{JL(77)}l_7^2\right)f(J,k)^2 + \left(H_v + l_{JL(77)}l_7^2\right)f(J,k)^3\end{aligned} \tag{2}$$

where G_v is the pure vibrational energy, B_v is the rotational constant, and D_v and H_v are the quartic and sextic centrifugal distortion constants, respectively, of the vibrational state v. The dependence of these four constants on the vibrational angular momentum l_7 is expressed by the terms $\chi_{L(77)}$, $d_{JL(77)}$, $h_{JL(77)}$, and $l_{JL(77)}$.

As far as the vibrational l-type doubling term is concerned, the elements with $|\Delta k| = 2$ can be written as:

$$\begin{aligned}&\langle l_7 \pm 2, k \pm 2|H_{l-type}|l_7, k\rangle \\ &= \frac{1}{4}\left[q_7 + q_{7J}J(J+1) + q_{7JJ}J^2(J+1)^2\right] \times \sqrt{(v_7 \mp l_7)(v_7 \pm l_7 + 2)} \\ &\times\sqrt{f_{\pm 2}(J,k)}\end{aligned} \tag{3}$$

The functions $f(J,k)$ and $f_{\pm n}(J,k)$ appearing in the equations above are defined as follows:

$$f(J,k) = J(J+1) - k^2, \tag{4}$$

$$f_{\pm n}(J,k) = \prod_{p=1}^{n} J(J+1) - \left[k \pm (p-1)\right](k \pm p). \tag{5}$$

3.2 Spectral Features

The stretching bands ν_1, ν_2, and ν_3 are located between 1,900 and 3,400 cm^{-1} (2.9–5.3 μm), for both DC_3N and HC_3N. An overview of the vibrational bands recorded in this work is provided in **Figure 1**. By inspecting this figure, it is evident that all the twelve bands observed and analyzed show the typical contour of $\sum - \sum$ or $\Pi - \Pi$ bands of a linear rotor, thus presenting well-defined P and R branches, but no Q branch.

While the absolute intensities of DC_3N bands are quite similar to each other (ν_1 = 81 atm^{-1} cm^{-2}, ν_2 = 50 atm^{-1} cm^{-2}, and ν_3 = 39 atm^{-1} cm^{-2} Bénilan et al., 2006), the situation is different for HC_3N (ν_1 = 249 atm^{-1} cm^{-2}, ν_2 = 41 atm^{-1} cm^{-2}, and ν_3 = 8 atm^{-1} cm^{-2} Jolly et al., 2007), with an overall variation of more than one order of magnitude. Furthermore, the hot-bands analyzed in this work ($\nu_1 + \nu_7 - \nu_7$, $\nu_2 + \nu_7 - \nu_7$, and $\nu_3 + \nu_7 - \nu_7$) are nearly three times weaker than the corresponding fundamental bands because of the Boltzmann factor at room temperature (the energy of the $\nu_7 = 1$ state is 221.8 cm^{-1}). As stated in **Section 2.1**, spectral recordings were performed employing various pressure values to account for these different band intensities, and to obtain a homogeneous S/N ratio for a wide range of J values.

[1]Tamassia et al., 2021, in preparation

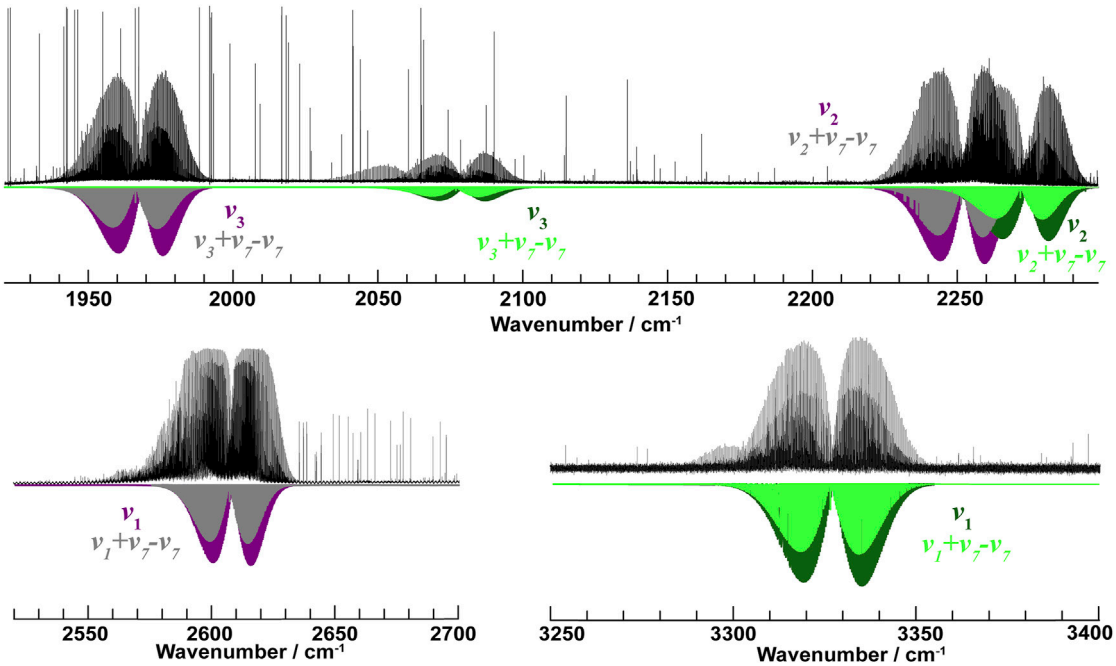

FIGURE 1 | Portions of the recorded MIR spectra (black traces): 1,930–2,300 cm^{-1}, 2,500–2,700 cm^{-1} and 3,250–3,400 cm^{-1}. Spectral simulations based on the spectroscopic constants of **Tables 2**, **3** are reported for both DC_3N (violet traces) and HC_3N (green traces). Recording conditions: T = 298 K, p = 16–32 Pa (top and bottom-left: 32 Pa, bottom-right: 16 Pa), L_{opt} = 8 m, 140–200 scans, unapodized resolution 0.004 cm^{-1}.

In addition to the infrared measurements, pure rotational spectra of three vibrational excited states of DC_3N were recorded between 243 and 295 GHz using the spectrometer described in **Section 2.2**. In detail: some $J + 1 \leftarrow J$ rotational transitions have been observed for the $\nu_3 = 1$, $\nu_2 = 1$, and $\nu_3 = \nu_7 = 1$ states, with J ranging from 28 to 34. Both $\nu_3 = 1$ and $\nu_2 = 1$ are $\sum$ states and their rotational spectra appear like a sequence of (almost) equally-spaced lines, while the $\nu_3 = \nu_7 = 1$ state has a $\prod$ symmetry, thus showing a series of doublets due to the l type resonance.

3.3 Analysis of the Spectra

The analysis of the ro-vibrational and pure rotational spectra has been performed with the aid of the PGOPHER program (Western, 2017) and the CALPGM suite (Pickett, 1991). Initially, more than 1500 ro-vibrational transitions of DC_3N belonging to the fundamental bands ν_1, ν_2, and ν_3 and to their hot-bands $\nu_1 + \nu_7 - \nu_7$, $\nu_2 + \nu_7 - \nu_7$, and $\nu_3 + \nu_7 - \nu_7$ were assigned, and they include high-J transitions up to $J = 110$. However, not all the ro-vibrational transitions assigned could be incorporated in the fit with the estimated experimental accuracy. In particular, the $\nu_2 + \nu_7 - \nu_7$ hot-band exhibited some deviations from our modelling, especially for transitions with J between 10 and 15. To check and correct possible misassignments, we have also employed the Loomis-Wood for Windows (LWW) program package for symmetric-top molecules (Łodyga et al., 2007), which revealed no errors in our assignments, through both the graphical diagrams and the Ground State Combination Differences (GSCDs) method. Possible perturbations due to a nearby state are therefore plausible. However, the identification of the perturbing state is not feasible at these energies because of the very large number of unknown ro-vibrational levels. Since a complete treatment of all the anharmonic resonances is beyond the goal of this work, an effective approach has been adopted and lines showing the largest deviations (10 in total) were removed from the analysis. The comparison between the simulation based on our analysis and the observed $\nu_2 + \nu_7 - \nu_7$ ro-vibrational transitions is shown in **Figure 2**, together with the corresponding Loomis-Wood plot.

The analysis of the other five bands was instead rather straightforward and satisfactory, with the Hamiltonian of **Eqs 1–3** able to well reproduce all experimental data within their nominal uncertainty. The quality of the band analyses can be inferred from the root-mean-square (rms) errors of the fits, which are reported in **Table 1**.

The spectroscopic constants determined from the preliminary analysis of the six bands of DC_3N were used to predict its pure rotational spectrum in the $\nu_3 = 1$, $\nu_2 = 1$, and $\nu_3 = \nu_7 = 1$ states, which are the three lowest energy states among those investigated in this work. A total of 21 pure rotational transitions, which do not suffer from contamination of nearby lines, have been successfully recorded and then added to the data-set in order to improve the accuracy of the spectroscopic parameters determined in the fit. It should be pointed out that, although the analysis of the ν_3 band gave no hint of perturbations (as evident from its LWW plot in **Figure 3**) and the fit has a rms error as low as 3.4×10^{-4} cm^{-1}, the rotational transitions recorded in the $\nu_3 = 1$ state show deviations about 10 times larger than the expected error, i.e., around 300 kHz. Once again, a plausible

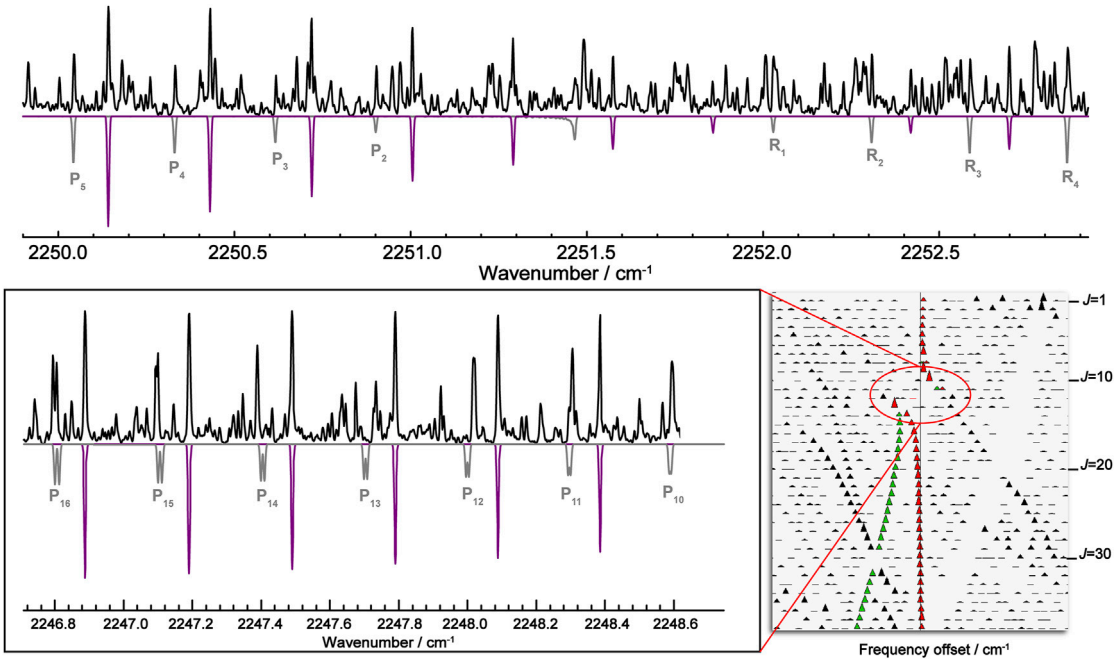

FIGURE 2 | (Top panel): Portions of the $\nu_2 + \nu_7 - \nu_7$ band of DC_3N. Recording conditions: T = 298 K, p = 32 Pa, L_{opt} = 8 m, 200 scans, unapodized resolution 0.004 cm^{-1}. **(Bottom panel)**: Detail of the spectrum **(left)** together with its Loomis-Wood plot **(right)** where the strongest perturbations are visible. Additional lines present in the spectra arise from other hot-bands, which will be targeted in future studies.

TABLE 1 | Summary of the ro-vibrational bands recorded and analyzed in this work.

Species	Band	Sub-band	J max	Freq. Range (cm^{-1})	Lines	rms error (10^{-4} cm^{-1})
DC_3N						
	ν_1	$\Sigma-\Sigma$	110	2,577–2,635	189	3.5
	ν_2	$\Sigma-\Sigma$	105	2,215–2,275	199	3.6
	ν_3	$\Sigma-\Sigma$	110	1,932–1,995	219	3.4
	$\nu_1 + \nu_7 - \nu_7$	$\Pi-\Pi$	100	2,579–2,632	269	6.3
	$\nu_2 + \nu_7 - \nu_7$	$\Pi-\Pi$	91	2,220–2,271	284	20.3
	$\nu_3 + \nu_7 - \nu_7$	$\Pi-\Pi$	97	1,943–1,990	292	4.1
HC_3N						
	ν_1	$\Sigma-\Sigma$	91	3,298–3,352	174	5.0
	ν_2	$\Sigma-\Sigma$	91	2,243–2,296	161	4.0
	ν_3	$\Sigma-\Sigma$	87	2,050–2,102	169	3.7
	$\nu_1 + \nu_7 - \nu_7$	$\Pi-\Pi$	78	3,301–3,348	225	6.0
	$\nu_2 + \nu_7 - \nu_7$	$\Pi-\Pi$	93	2,249–2,294	240	4.3
	$\nu_3 + \nu_7 - \nu_7$	$\Pi-\Pi$	71	2,052–2,096	252	4.0

explanation is that the ν_3 = 1 state is involved in an anharmonic interaction with one or more vibrational states close in energy, but such perturbation is moderately weak and hidden in the larger uncertainty of the infrared data. Nonetheless, despite these somewhat large residuals, the inclusion of pure rotational lines reduces the uncertainty of the derived spectroscopic parameters by up to a factor of 3. The upper states spectroscopic parameters determined from the combined analysis of rotational and ro-vibrational transitions are collected in **Table 2**. The spectroscopic constants of the ground and ν_7 = 1 states, i.e., the lower levels involved in the current analysis, were kept fixed at the values determined in our previous global analysis (see Tables 4, 5 in Melosso et al., 2020).

As far as HC_3N is concerned, being a side-product of our spectral recording, we limited the analysis to its infrared spectrum. With the only exception of a few small deviations involving blocks of 2–3 consecutive J levels, no evident perturbations were observed during the assignment procedure and/or at the fitting stage. Overall, for HC_3N, 1221 different lines were assigned to the ν_1, ν_2, and ν_3 fundamental bands and their corresponding hot bands originating from the ν_7 = 1 state. Similarly to DC_3N, the vibrational energies G_v and the

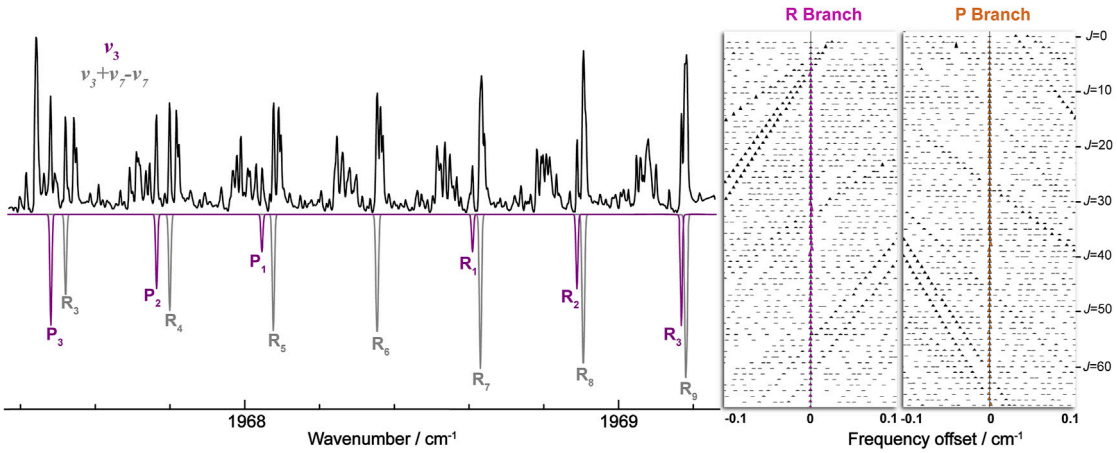

FIGURE 3 | (Left panel): Portions of the DC_3N spectrum in the region of the ν_3 band system. Recording conditions: same as **Figure 2**. **(Right panel)**: Loomis-Wood plots of the P and R branches of the ν_3 band. Additional lines present in the spectra arise from other hot-bands, which will be targeted in future studies.

TABLE 2 | Spectroscopic constants determined for DC_3N.

Constant	Unit	$v_1 = 1$	$v_2 = 1$	$v_3 = 1$	$v_1 = v_7 = 1$	$v_2 = v_7 = 1$	$v_3 = v_7 = 1$
G_v	cm^{-1}	2,608.5183 (2)	2,252.1388 (1)	1,968.3280 (1)	2,818.8187 (1)	2,463.0161 (1)	2,177.9480 (1)
χ_{77}	GHz				19.5125[a]	19.5125[a]	19.5125[a]
B_v	MHz	4,210.218 (5)	4,203.792 (2)	4,209.911 (2)	4,223.177 (2)	4,216.951 (3)	4,222.925 (2)
D_v	kHz	0.445 (1)	0.4555 (7)	0.4541 (5)	0.4678 (3)	0.4583 (4)	0.4757 (8)
H_v	mHz	0.14 (7)	0.39 (5)	0.15 (4)	0.0394[b]	0.0394[b]	0.0394[b]
d_{J77}	kHz				−9.971[a]	−9.971[a]	−9.971[a]
q_7	MHz				5.900 (3)	5.129 (3)	5.942 (2)
q_{J7}	Hz				−12.3 (4)	−25.4 (6)	−13.9 (3)

[a]*Fixed at the $v_7 = 1$ value (Melosso et al., 2020).*
[b]*Fixed at the ground state value (Melosso et al., 2020).*
Notes: Numbers in parentheses represent 1σ errors in units of the last significant digit.

TABLE 3 | Spectroscopic constants determined for HC_3N.

Constant	Unit	$v_1 = 1$	$v_2 = 1$	$v_3 = 1$	$v_1 = v_7 = 1$	$v_2 = v_7 = 1$	$v_3 = v_7 = 1$
G_v	cm^{-1}	3,327.37141 (7)	2,273.99485 (7)	2,079.30610 (7)	3,548.40903 (7)	2,493.65068 (6)	2,298.77771 (8)
χ_{77}	GHz				21.7972[a]	21.7972[a]	21.7972[a]
B_v	MHz	4541.774 (2)	4,527.493 (2)	4,535.116 (2)	4,556.205 (2)	4,541.989 (1)	4,549.738 (5)
D_v	kHz	0.5401 (2)	0.5380 (2)	0.5412 (3)	0.5542 (3)	0.5608 (2)	0.569 (3)
H_v	mHz	0.0509[b]	0.0509[b]	0.0509[b]	0.0509[b]	0.0509[b]	0.0509[b]
d_{J77}	kHz				−12.287[a]	−12.287[a]	−12.287[a]
q_7	MHz				6.543 (2)	6.650 (2)	6.457 (3)
q_{J7}	Hz				−17.3 (5)	−18.3 (3)	−14.9 (7)

[a]*Fixed at the $v_7 = 1$ value (Bizzocchi et al., 2017).*
[b]*Fixed at the ground state value (Bizzocchi et al., 2017).*
Notes: Numbers in parentheses represent 1σ errors in units of the last significant digit.

rotational constants B_v were determined with high precision for all the six vibrational excited states. Accurate values for the centrifugal distortion constant D_v and the *l*-type doubling constant q_7 were derived as well. **Table 3** lists the complete set of upper state spectroscopic parameters used in the final fit, while the quality of the analysis is demonstrated by the low rms error achieved for each band (see **Table 1**). Also in this case, the spectroscopic constants of the ground and $v_7 = 1$ states were kept fixed at the values determined in our previous global analysis (see Table 5 in Bizzocchi et al., 2017).

The fit output files containing the assigned transitions, their wavenumbers, and the residual errors for each band are provided as **Supplementary Material**.

4 DISCUSSION AND CONCLUSION

Nowadays, the improvement of the ground-based infrared facilities (e.g., CRIRES + at VLT) and the perspectives opened by the forthcoming JWST telescope (with MIRI and NISPEC instruments) have brought a considerable interest to the ro-vibrational spectrum of simple interstellar molecules, both at low and high wavenumbers. In particular, the possibility of probing the inner portions of young proto-planetary disks where the material is funneled into the planetary formation zone and—at later stages—to directly observe the atmospheres of the mature exoplanets, makes the stretching spectral interval (1,500–3,500 cm^{-1}) of particular interest due to its selectivity to the high gas temperatures typical of these regions. In this context, a detailed knowledge of the associated hot bands is as important as that of the fundamentals. In high excitation conditions, many vibrational states are significantly populated and the corresponding satellite features are able to make up a considerable amount of the retrieved flux. Hot bands are thus critical to accurately model the shape of the band profile and to retrieve reliable column densities. The laboratory detection of accurate infrared spectra is therefore essential to guide such astronomical investigations. Prior to our investigation, the knowledge of the mid-infrared spectra of DC_3N and HC_3N above 1,200 cm^{-1} was sparse and deficient in terms of measurement precision.

Therefore, part of the MIR spectra of DC_3N and HC_3N has been re-investigated with a FTIR spectrometer, which ensures high-resolution across a broad band spectrum. Three fundamentals (ν_1, ν_2, and ν_3) and three hot bands ($\nu_1 + \nu_7 - \nu_7$, $\nu_2 + \nu_7 - \nu_7$, and $\nu_3 + \nu_7 - \nu_7$) have been recorded and analyzed for each species. Thanks to the high resolution of the spectrometer employed, an accuracy of about 5×10^{-4} cm^{-1} has been achieved in terms of line positions, and the splittings due to the *l*-type resonance in Π states could be resolved for most of the transitions. Due to the relatively high Doppler broadening at these frequencies (4–5 $\times$ 10^{-3} cm^{-1}), a higher instrumental resolution is not sufficient to achieve a higher accuracy of the spectroscopic parameters. Such limitation can be overcome only in Doppler-free conditions, e.g., working in the saturation regime (Diouf et al., 2019; Hua et al., 2019).

Additional and complementary measurements were performed with a FM millimeter/submillimeter-wave spectrometer, equipped with a furnace that allowed to record pure rotational transitions in highly excited states (with energies above 2,000 cm^{-1}). The inclusion of rotational lines, whose precision is intrinsically much higher than ro-vibrational data, led to an improved determination of the upper state spectroscopic parameters. If compared to the previous work, our constants are more than two orders of magnitude more accurate than those from Mallinson and Fayt (1976), and are consistent with the most recent spectroscopic data available for DC_3N (Melosso et al., 2020) and HC_3N (Bizzocchi et al., 2017). Additionally, the line list for the $\nu_2 + \nu_7 - \nu_7$ hot-band reported by Mallinson and Fayt (1976) in their Supplementary Material appears to be wrong and inconsistent with the spectroscopic constants they reported in the paper. Such a misassignment has been corrected in this work. The new set of spectroscopic constants, in combination with the absolute intensity values derived by Bénilan et al. (2006); Jolly et al. (2007), can now be used to produce accurate line catalogs for the ν_1, ν_2, and ν_3 band systems of both DC_3N and HC_3N. However, a full modeling of the MIR spectra of these species would require the analysis of additional features, i.e., combination, overtone, and hot-bands (Mallinson and Fayt, 1976; Bénilan et al., 2006; Jolly et al., 2007). Future studies will focus on these subjects.

As a final remark, the high-temperature rotational spectroscopy experimental technique presented in this work can be successfully applied to future investigations of the vibrational excited states of molecules relevant to astrophysics and possessing only highly-energetic vibrations, such as water or other small species.

DATA AVAILABILITY STATEMENT

The original contributions presented in the study are included in the article/**Supplementary Material**, further inquiries can be directed to the corresponding author.

AUTHOR CONTRIBUTIONS

MM, FT, and CP contributed to conception and design of the study; JG synthesized the sample; MM, FT, and LD set-up the experiments; NJ, MM, FT, and EC recorded the spectra; NJ prepared the figures; MM organized the tables; NJ, MM, and FT performed the analysis; NJ wrote the first draft of the article with the help of MM and CP; MM, LB, and CP wrote sections of the article; DF contributed to the discussion on the astronomical applications. All authors contributed to article revision, read, and approved the submitted version.

FUNDING

This study was supported by Bologna University (RFO funds) and by MIUR (Project PRIN 2015: STARS in the CAOS, Grant Number 2015F59J3R). NJ thanks the China Scholarships Council (CSC) for the financial support. JG thanks the Centre National d'Etudes Spatiales (CNES) for a grant. The paper is published with the contribution of the Department of Excellence program financed by the Ministry of Education, University and Research (MIUR, L. 232 del 01/12/2016).

SUPPLEMENTARY MATERIAL

The Supplementary Material for this article can be found online at: https://www.frontiersin.org/articles/10.3389/fspas.2021.656295/full#supplementary-material.

REFERENCES

Banks, K., Larson, M., Aymergen, C., and Zhang, B. (2008). "James webb space telescope mid-infrared instrument cooler systems engineering," in *Modeling, systems engineering, and project management for astronomy III*, Editors George, Z. A., and Martin, J. C. (Bellingham, WA: International Society for Optics and Photonics), 7017, 70170A.

Belloche, A., Müller, H. S. P., Garrod, R. T., and Menten, K. M. (2016). Exploring molecular complexity with ALMA (EMoCA): deuterated complex organic molecules in Sagittarius $B_2(N_2)$. *Astron. Astrophys.* 587, A91. doi:10.1051/0004-6361/201527268

Bénilan, Y., Jolly, A., Raulin, F., and Guillemin, J.-C. (2006). IR band intensities of DC_3N and $HC_3{}^{15}N$: implication for observations of Titan's atmosphere. *Planet. Space Sci.* 54, 635–640. doi:10.1016/j.pss.2006.01.006

Bizzocchi, L., Tamassia, F., Laas, J., Esposti, C. D., Dore, L., Melosso, M., et al. (2017). Rotational and high-resolution infrared spectrum of HC_3N: global ro-vibrational analysis and improved line catalog for astrophysical observations. *Astrophys. J. Suppl. Ser.* 233, 11. doi:10.3847/1538-4365/aa9571

Ceccarelli, C., Caselli, P., Bockelée-Morvan, D., Mousis, O., Pizzarello, S., Robert, F., et al. (2014). "Deuterium fractionation: the ariadne's thread from the precollapse phase to meteorites and comets today," in *Protostars and Planets VI*, 859–882. doi:10.2458/azu_uapress_9780816531240-ch037

Diouf, M. L., Cozijn, F. M. J., Darquié, B., Salumbides, E. J., and Ubachs, W. (2019). Lamb-dips and lamb-peaks in the saturation spectrum of hd. *Opt. Lett.* 44, 4733–4736. doi:10.1364/ol.44.004733

Dore, L., Bizzocchi, L., and Degli Esposti, C. (2012). Accurate rotational rest-frequencies of CH2NH at submillimetre wavelengths. *Astron. Astrophys.* 544, A19. doi:10.1051/0004-6361/201219674

Esplugues, G. B., Cernicharo, J., Viti, S., Goicoechea, J. R., Tercero, B., Marcelino, N., et al. (2013). Combined IRAM and Herschel/HIFI study of cyano(di) acetylene in Orion KL: tentative detection of DC_3N. *Astron. Astrophys.* 559, A51. doi:10.1051/0004-6361/201322073

Gordon, I. E., Rothman, L. S., Hill, C., Kochanov, R. V., Tan, Y., Bernath, P. F., et al. (2017). The HITRAN2016 molecular spectroscopic database. *J. Quant. Spectrosc. Ra.* 203, 3–69. doi:10.1016/j.jqsrt.2017.06.038

Howe, D. A., Millar, T. J., Schilke, P., and Walmsley, C. M. (1994). Observations of deuterated cyanoacetylene in dark clouds. *Mon. Not. R. Astron. Soc.* 267, 59–68. doi:10.1093/mnras/267.1.59

Hua, T. P., Sun, Y. R., Wang, J., Liu, A. W., and Hu, S. M. (2019). Frequency metrology of molecules in the near-infrared by nice-ohms. *Opt. Express* 27, 6106–6115. doi:10.1364/oe.27.006106

Jolly, A., Benilan, Y., and Fayt, A. (2007). New infrared integrated band intensities for HC_3N and extensive line list for the ν_5 and ν_6 bending modes. *J. Mol. Spectrosc.* 242, 46–54. doi:10.1016/j.jms.2007.01.008

Langer, W. D., Schloerb, F. P., Snell, R. L., and Young, J. S. (1980). Detection of deuterated cyanoacetylene in the interstellar cloud TMC 1. *Astrophys. J.* 239, L125–L128. doi:10.1086/183307

Łodyga, W., Kreglewski, M., Pracna, P., and Urban, Š. (2007). Advanced graphical software for assignments of transitions in rovibrational spectra. *J. Mol. Spectrosc.* 243, 182–188. doi:10.1016/j.jms.2007.02.004

Mallinson, P. D., and Fayt, A. (1976). High resolution infra-red studies of HCCCN and DCCCN. *Mol. Phys.* 32, 473–485. doi:10.1080/00268977600103231

McGuire, B. A. (2018). 2018 census of interstellar, circumstellar, extragalactic, protoplanetary disk, and exoplanetary molecules. *Astrophys. J. Suppl. S.* 239, 17. doi:10.3847/1538-4365/aae5d2

Melosso, M., Bizzocchi, L., Adamczyk, A., Canè, E., Caselli, P., Colzi, L., et al. (2020). Extensive ro-vibrational analysis of deuterated-cyanoacetylene (DC_3N) from millimeter-wavelengths to the infrared domain. *J. Quant. Spectrosc. Radiat. Transf.* 254, 107221. doi:10.1016/j.jqsrt.2020.107221

Melosso, M., Bizzocchi, L., Tamassia, F., Degli Esposti, C., Canè, E., and Dore, L. (2019a). The rotational spectrum of ^{15}ND. Isotopic-independent Dunham-type analysis of the imidogen radical. *Phys. Chem. Chem. Phys.* 21, 3564–3573. doi:10.1039/c8cp04498h

Melosso, M., Conversazioni, B., Esposti, C. D., Dore, L., Cané, E., Tamassia, F., et al. (2019b). The pure rotational spectrum of $^{15}ND_2$ observed by millimetre and submillimetre-wave spectroscopy. *J. Quant. Spectrosc. Radiat. Transf.* 222, 186–189. doi:10.1016/j.jqsrt.2018.10.028

Pickett, H. M. (1991). The fitting and prediction of vibration-rotation spectra with spin interactions. *J. Mol. Spectrosc.* 148, 371–377. doi:10.1016/0022-2852(91)90393-o

Rivilla, V. M., Colzi, L., Fontani, F., Melosso, M., Caselli, P., Bizzocchi, L., et al. (2020). DC_3N observations towards high-mass star-forming regions. *Mon. Not. R. Astron. Soc.* 496, 1990–1999. doi:10.1093/mnras/staa1616

Stoppa, P., Tasinato, N., Baldacci, A., Charmet, A. P., Giorgianni, S., Tamassia, F., et al. (2016). FTIR spectra of CH2F2 in the 1000–1300 cm^{-1} region: rovibrational analysis and modeling of the Coriolis and anharmonic resonances in the ν_3, ν_5, ν_7, ν_9 and $2\nu_4$ polyad. *J. Quant. Spectrosc. Ra.* 175, 8–16. doi:10.1016/j.jqsrt.2016.01.035

Tamassia, F., Melosso, M., Dore, L., Pettini, M., Canè, E., Stoppa, P., et al. (2020). Spectroscopy of a low global warming power refrigerant. Infrared and millimeter-wave spectra of trifluoroethene (HFO-1123) in the ground and some vibrational excited states. *J. Quant. Spectrosc. Ra.* 248, 106980. doi:10.1016/j.jqsrt.2020.106980

Western, C. M. (2017). PGOPHER: a program for simulating rotational, vibrational and electronic spectra. *J. Quant. Spectrosc. Radiat. Transf.* 186, 221–242. doi:10.1016/j.jqsrt.2016.04.010

Yamada, K., Best, R., and Winnewisser, G. (1983). Diode laser spectrum of HCCCN: CN stretching band. *Z. Naturforsch. A.* 38, 1296–1308. doi:10.1515/zna-1983-1205

Yamada, K., Schieder, R., Winnewisser, G., and Mantz, A. W. (1980). Diode laser spectrum of HCCCN near 5 μm. *Z. Naturforsch. A.* 35, 690–693. doi:10.1515/zna-1980-0705

Yamada, K., and Winnewisser, G. (1981). Diode laser spectrum of HCCCN near 5 μm. The hot band. *Z. Naturforsch. A.* 36, 23–29. doi:10.1515/zna-1981-0105

Conflict of Interest: The authors declare that the research was conducted in the absence of any commercial or financial relationships that could be construed as a potential conflict of interest.